Molecular Simulation

ISSN: 0892-7022 (Print) 1029-0435 (Online) Journal homepage: www.tandfonline.com/journals/gmos20

Molecular dynamics simulations of noble gases encapsulated in C_{60} Fullerene

W. Even, J. Smith & M.W. Roth

To cite this article: W. Even, J. Smith & M.W. Roth (2005) Molecular dynamics simulations of noble gases encapsulated in C_{60} Fullerene, Molecular Simulation, 31:4, 207-213, DOI: 10.1080/08927020412331332767

To link to this article: https://doi.org/10.1080/08927020412331332767

Published online: 19 Aug 2006.

Molecular Simulation, Vol. 31, No. 4, 15 April 2005, 207–213

Taylor & Francis
Taylor & Francis Group

Molecular dynamics simulations of noble gases encapsulated in C_{60} Fullerene

W. EVEN†, J. SMITH‡ and M.W. ROTH¶*

†Department of Physics and Astronomy, Louisiana State University, Baton Rouge, LA 70803-4001, USA
‡Present address: Sandia National Laboratories, Albuquerque, NM 87185, USA
¶Department of Physics, University of Northern Iowa, Cedar Falls, IA 50614, USA

(Received October 2004; in final form November 2004)

Molecular dynamics simulations of Helium (He), Neon (Ne), Argon (Ar), Krpton (Kr) and Xenon (Xe) encapsulated in C_{60} are discussed, as well simulations of Fullerenes containing anywhere from two to four He atoms. Even for single atom encapsulates, no species resides at the geometric center of the Fullerene cage. Smaller atoms sit more off-center than larger ones, and He appears to be a special case in both centering and dynamics. Some encapsulated species stabilize the cage by stifling radial fluctuations and others disrupt it; adding Ne seems to have the most stabilizing effect, while Kr and Xe cause the largest radial atomic excursions. Multiple He encapsulates tend to stabilize the cage; such systems are very stressed and show structure over a wide temperature range. Based on dynamical information quadruple He seems to be close to the packing limit for C_{60}.

Keywords: Endohedral fullerenes; Molecular dynamics; Noble gases; Encapsulation

1. Introduction

Since their discovery nearly 20 years ago, Fullerenes have been of intense scientific interest. Of the many new phenomena presented by systems that include Fullerenes, encapsulation is doubtless one of the most influential and far-reaching. As an example, helium isotopes may be trapped in extraterrestrial objects or even on the ancient earth such that unique isotope ratios of the encapsulated species are preserved and information about the environment or time of formation may be gained [1]. Helium (He), Neon (Ne), Argon (Ar), Krypton (Kr) and Xenon (Xe) have been placed within Fullerenes using either formation in an ambient rare gas environment, high-pressure intrusion, collisions or products of nuclear reactions [2,3]. It was originally a surprise that even Xe could be incorporated into C_{60} [4], as its Van der Waals radius approximates that of the cage vacancy. NMR spectroscopy is used for further study in the cases of ^{3}He and ^{129}Xe [2–4]. The mechanism for encapsulation is still poorly understood. However, utilization of catalyst such as HCN increases incorporation and yield considerably [5], suggesting that the local environment of the Fullerene cage is of considerable importance chemically as well as physically. More than one encapsulated species may be present within a Fullerene cavity, resulting in "molecules" such as He_2 [6], Ne_2 [7] and HeKr [8]. In fact, di-helium [6] has been encapsulated in both C_{70} as well as C_{60}, and has been studied in order to elucidate information about the Fullerene hexanion magnetic fields.

In addition to ongoing experimental efforts, computational studies can lend considerable insight into the dynamical processes exhibited by Fullerene systems. In fact, different mechanisms for encapsulation [2,3] and even release [1] have been proposed and studied computationally [9,10]. Deterministic computer simulations are also used to examine various phase transitions of Fullerenes [11], their melting [12], thermal disintegration [13], fragmentation from collisions [14] and physisorption onto them [15]. Extensive molecular dynamics (MD) simulations of the Fullerene formation process from the vapor phase [16–20] show that monocyclic rings, polycyclic structures and even C_{40}-C_{70} closed cages can coalesce from the carbon vapor phase. In such simulations, a Verlet algorithm is used with temperature control over translational, rotational and

*Corresponding author. Tel.: +1-319-273-7336. Fax: +1-319-273-7136. E-mail: rothm@uni.edu

Molecular Simulation
ISSN 0892-7022 print/ISSN 1029-0435 online © 2005 Taylor & Francis Group Ltd
http://www.tandf.co.uk/journals
DOI: 10.1080/08927020412331332767

vibrational degrees of molecular freedom, and a form of the Brenner bonded carbon–carbon potential [21] describes the atomic C—C bonded interactions. The Fullerene formation simulations seem particularly noteworthy because of the wide range of closed structures appearing from such disordered initial conditions.

Since several encapsulated noble gases actually exist, they comprise an ideal group over which systematic comparisons may be made. It is thought that the electronic structure of Xe (and its cage) are considerably altered through encapsulation; however in light of the fact that rare gases do not bond to the cage as well as the successes of many MD simulation techniques in describing important dynamical aspects of Fullerene systems, classical simulations seem somewhat relevant. We would like to add to the understanding of the behavior of endohedral noble gas systems, so we conduct MD simulations of He, Ne, Ar, Kr and Xe encapsulated in C_{60} Fullerene. Specifically, the purpose of this study is to systematically compare the behavior of different systems across the rare gases, to better understand the effect that encapsulation has on the cage, and to investigate the behavior of noble gas "molecules" that are formed by encapsulation of multiple He atoms.

2. Computational approach

We employ an (N, V, T) MD method to simulate the behavior of various rare gases encapsulated within C_{60}. There is initially one rare gas atom placed at the center of the Fullerene. As the simulation proceeds, the equations of motion are integrated using a standard Verlet algorithm with a time step $\Delta t = 0.0005$ ps, and various quantities of interest are calculated. Any center-of-mass motion of the Fullerene is subtracted off as the simulation proceeds. Spurious rotational motion of the Fullerene is also accounted for in a similar way, only using its moment of inertia tensor and angular momentum. Temperature control is achieved by velocity rescaling for the entire system in the case of empty cages and single atom encapsulates, and separately for the Fullerene cage and He in the case of multiple encapsulated He atoms. Runs are started with an equilibrated Fullerene and taken out to 10^6 time steps (500 ps).

There are several types of interaction potentials used in the simulations. The rare gas-rare gas potential as well as the rare gas–Carbon potential are of a Lennard–Jones form,

$$u_{\mathrm{LJ}}(r_{ij}) = 4\varepsilon_{ij}\left[\left(\frac{\sigma_{ij}}{r_{ij}}\right)^{12} - \left(\frac{\sigma_{ij}}{r_{ij}}\right)^{6}\right], \tag{1}$$

where the potential parameters between various species are given in Table 1; mixed interaction parameters are obtained with the use of Lorentz–Bertholot combining rules. In addition there is a non-bonded carbon–carbon interaction [22] which is in a modified Lennard–Jones form whose parameters are also shown in Table 1:

$$u_{\mathrm{LJ}}(r_{ij}) = \varepsilon_{\mathrm{CC}}\left[\left(\frac{\sigma_{\mathrm{CC}}}{r_{ij}}\right)^{12} - 2\left(\frac{\sigma_{\mathrm{CC}}}{r_{ij}}\right)^{6}\right]. \tag{2}$$

The carbon–carbon bonded interactions are modeled by Brenner's empirical extended bond-order potential [21]

$$\left.\begin{aligned} V_R(r_{ij}) &= f(r_{ij})\tfrac{D_e}{S-1}\exp\left[-\beta\sqrt{2S}(r-R_e)\right] \\ V_A(r_{ij}) &= f(r_{ij})\tfrac{D_eS}{S-1}\exp\left[-\beta\sqrt{\tfrac{2}{S}}(r-R_e)\right] \\ f(r_{ij}) &= \begin{cases} 1, r \le R_1 \\ \frac{1}{2}\left[1+\cos\left(\frac{(r_{ij}-R_1)\pi}{(R_2-R_1)}\right)\right], R_1 \le r_{ij} \le R_2 \\ 0, r_{ij} \ge R_2 \end{cases} \end{aligned}\right\}, \tag{3a}$$

which has parameters that are fit to various energetics of hydrocarbons, diamond and graphite. In equations (3a), V_R and V_A are the repulsive and attractive terms, respectively, which are essentially modified Morse potentials. The screening function $f(r_{ij})$ restricts the interaction to nearest neighbors as defined by the values for $R_1$and R_2. In addition, the Brenner potential takes bonding topology into account with the empirical bond order function $\bar{B}_{ij}$ given by the relationships

$$\left.\begin{aligned} B_{ij} &= 1 + \left[\sum_{k\neq i,j}^{N} G_C(\theta_{ijk}) f(r_{ik})\right]^{-\delta} \\ G_C(\theta) &= a_0\left[1 + \tfrac{c_0^2}{d_0^2} - \tfrac{c_0^2}{d_0^2+(1+\cos\theta)^2}\right] \\ \bar{B}_{ij} &= \tfrac{B_{ij}+B_{ji}}{2} \end{aligned}\right\}. \tag{3b}$$

Here the three-body bond angle is defined as

$$\theta_{ijk} = \cos^{-1}\left(\frac{\vec{r}_{ji}\cdot\vec{r}_{jk}}{r_{ji}r_{jk}}\right), \tag{3c}$$

where $\vec{r}_{ab}$is the displacement vector from carbon atom a to carbon atom b. Variations of the Brenner potential have been used for many different types of carbon allotrope simulations, as the empirical bond order function controls

Table 1. Parameters for the non-bonded Lennard–Jones interaction potentials.

Species	$\varepsilon_{ij}(K)$	σ_{ij} (Å)
He–He	10.80	2.57
Ne–Ne	36.68	2.79
Ar–Ar	120.0	3.38
Kr–Kr	171.0	3.60
Xe–Xe	221.0	4.10
C–C*	28.0	3.4
C–C	34.839	3.805

The carbon–carbon parameters with the asterisk (*) are those for a standard Lennard–Jones potential as in equation 1 and are used for the purpose of calculating cross interaction terms for unlike species with the Lorentz–Bertholot combining rules. The carbon–carbon parameters without the asterisk are for a modified Lennard–Jones interaction as shown in equation 2, and are used in carbon–carbon nonbond interactions in the simulations [22].

Table 2. Parameters for the bonded carbon–carbon Brenner interaction potential.

Parameter	*Value*
D_e	73333.33 K
β	1.5 Å^{-1}
S	1.29
R_e	1.315 Å
R_1	1.750 Å
R_2	2.000 Å
δ	0.80469
a_0	0.011304
c_0	19
d_0	2.5

clustering to some extent. For example, Yamaguchi *et al.* [16–20] do not include information from the conjugate bond-order term B_{ji} because then the potential would not adequately apply to small clusters, but since we are dealing with complete Fullerenes, we include it. The entire carbon–carbon interaction is a sum over all bonded and non-bonded interactions:

$$u_{\mathrm{CC}} = \sum_{i=1}^{N} \sum_{j \geq i}^{N} \left\{ \left[V_R(r_{ij}) - \bar{B}_{ij} V_A(r_{ij}) \right] + P_{ij} u_{\mathrm{LJ}}(r_{ij}) \right\}. \quad (4)$$

Here P_{ij} is a screening function [22] which we implement by creating bonded and non-bonded neighbor lists. All carbon–carbon bonded potential parameters are given in Table 2.

3. Results and discussion

3.1 Single atom encapsulation

Figures 1 and 2 show radial distributions for the various rare gases inside C_{60} at different temperatures. Such distributions are the calculated probability that an atom resides at a certain distance range from r to $r + \Delta r$ from the geometrical center of the Fullerene cage. Although none of the atoms reside at the cage center, it is clear that He is a special case. Due to its low mass it is particularly sensitive to the highly inhomogeneous interaction potential it experiences with the Fullerene. It samples more of the space in the cavity with increasing temperature (shown by peak broadening) but does not necessarily show any clear trends in peak centering with changing temperature until high temperature ($T \approx 800$K) is reached. In contrast to He, larger atoms tend to reside closer to the center of the cage at a given temperature, and as temperature increases each one tends to move further off center, as peak positions indicate. Also, as temperature increases the larger atoms sample the cavity space considerably more smoothly than does He. It is interesting to note that the behavior of Ne is similar to that of Kr, and that Ar behaves somewhat like Xe. This is probably a result of the atoms seeking the lowest potential interaction spots given the constraints imposed by interplay of the size of the encapsulated species and the rough interaction potential inside the Fullerene.

The effect of encapsulation on the Fullerene cage is also monitored. Figure 3 shows bond angle distributions for the carbon atoms in the Fullerene cage with various encapsulated species at low temperature and at high temperature, including the empty cage. The bond angle distribution is calculated as the probability that a certain three-body bond angle (as defined in equation 3c) lies between θ_{ijk} and $\theta_{ijk} + \Delta\theta_{ijk}$. In addition, figure 4 shows carbon atom radial distributions for cases involving various encapsulated species at low temperature and at high temperature, and is calculated in a fashion similar to endohedral radial distributions, but only for the carbon atoms in the Fullerene cage. At low temperature, encapsulation has no significant effects on the cage. The bond-angle pentagon and hexagon peaks are distinct and almost coincident for various endohedral cases, and the peaks of the radial probability distribution show only slight differences. There appears to be no trend with atom type for either distribution although the curves for Ne@C_{60} are the most sharply peaked. We suspect, as before, that the slight differences observed are the results of the encapsulated species being under competing constraints. In contrast, examination of the radial character of the Fullerene at $T = 800$ K reveals that the presence of an encapsulated species can have a considerable effect on the cage, and certain trends are noticeable. The addition of He and Ne both stabilize the cage as compared to when it is empty, as the radial atomic distributions for both those encapsulates are more sharply peaked and the high radius shoulders starting at about 4.25 Å are less pronounced than for the empty cage. In fact, Ne gives the most stabilization against fluctuations, as the high radius shoulder starting at about 4.25 Å is entirely absent. Then, Ar, Kr and Xe show increasing disruption of the cage, as the central peaks of the radial atomic distributions become lower and the shoulder beginning at 4.25 Å increases dramatically. Whether a species disrupts or stabilizes the cage may be partly understood by considering the value of the Lennard–Jones encapsulate–carbon collision diameter σ in comparison to the Fullerene dimensions and the distance the atom spends from the Fullerene center. The smallest collision diameters cause the rare gas–carbon force to be attractive more often than not, while the largest parameters cause the potential to be repulsive, thus pushing carbon atoms away. For Ne—C, the collision diameter is about 3.1 Å giving a Ne—C equilibrium distance of about 3.5 Å. Taking the radial offset into account (figure 1) we see that the Ne—C separation is reasonably close to the equilibrium distance, but this is not the case for the other encapsulates. At high temperature, the pentagon and hexagon peaks in the bond-angle distribution have merged and such distributions show the same trends that the carbon radial distributions do as far as stabilization and disruption of the cage is concerned. It is interesting to note that the thermal disruption of the cage brought on by the presence of an encapsulated atom is mainly radial because, unlike the carbon radial distributions at $T = 800$K, the corresponding bond angle distribution

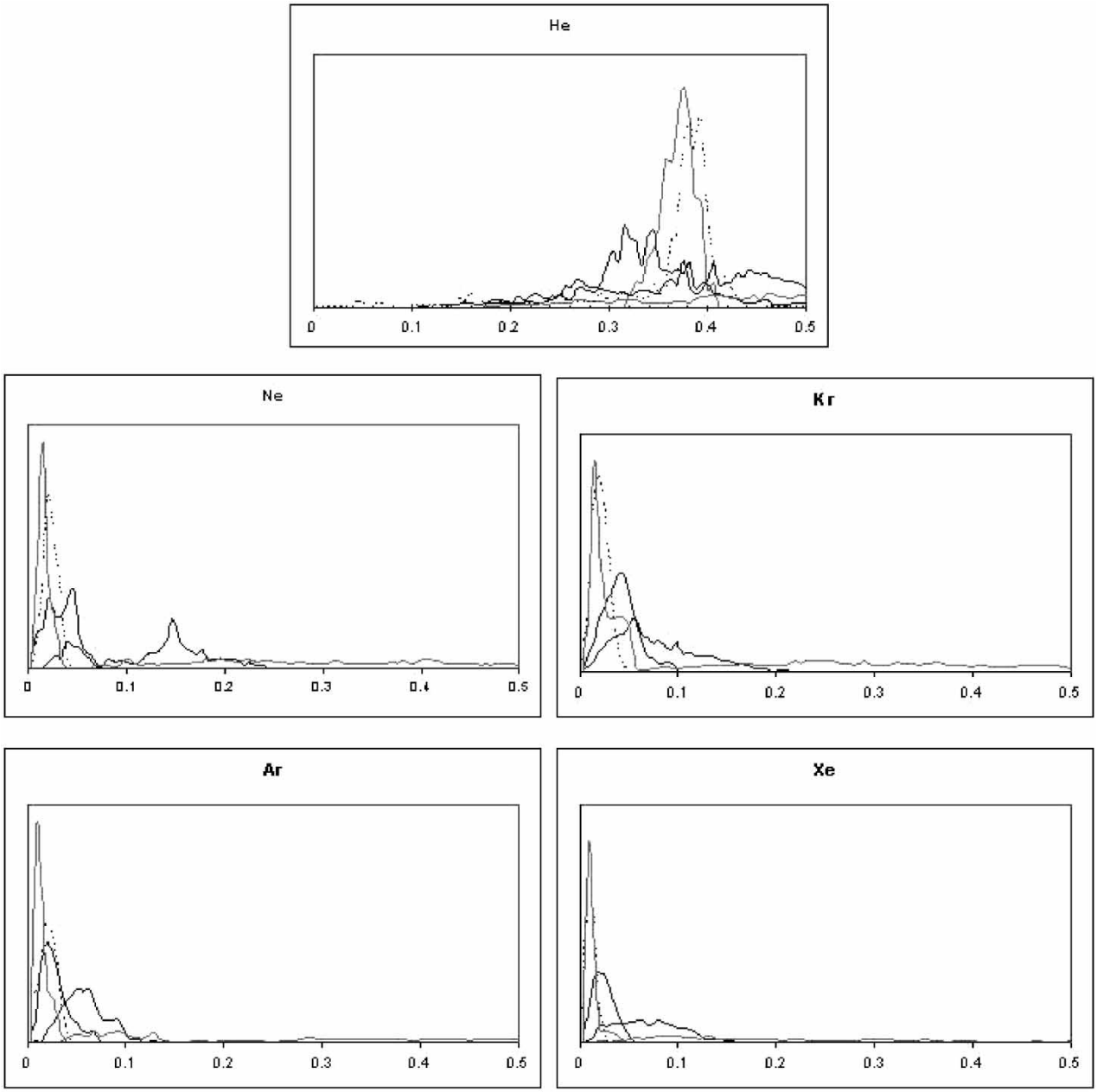

Figure 1. Radial distributions for He, Ne, Ar, Kr and Xe for $T = 160$ K (gray), 320 K (dashed), 480 K (regular black), 640 K (bold black) and 800 K (bold gray). Vertical axes are in arbitrary units and horizontal axes are atomic position in Ångstrom. All scales are identical. Distributions at $T = 800$ K are better represented in Figure 2.

shows no features significantly different from those with other encapsulates—even the empty cage. Such a result implies that, for the particular simulations being discussed here, the pentagon/hexagon rings in the cage are being preserved and no new type of cage disruption mechanism involving bond-orientational order removal is being introduced by an encapsulated species. From an energetic point of view, it is much easier to incur small radial disruptions of the cage as opposed to altering its bond-orientational order.

All the single atom encapsulation results presented here must be interpreted with one important caveat. Temperature control is achieved by velocity rescaling for the entire system. Since temperature is inherently a statistical quantity, speaking of the "temperature" of the noble gas encapsulate itself means nothing. Rather, the temperatures quoted here simply reflect information about the average kinetic energy of the system as a whole and we permit the interactions to dictate how kinetic energy is partitioned.

3.2 Multiple atom encapsulation

We also conduct simulations with 2, 3 and 4 He atoms inside C_{60}. Figure 5 shows radial distributions of the encapsulated atoms at various temperatures for various numbers of atoms. As for the single atom case, the radial distribution is the probability that an atom resides at a certain distance range from r to $r + \Delta r$ from

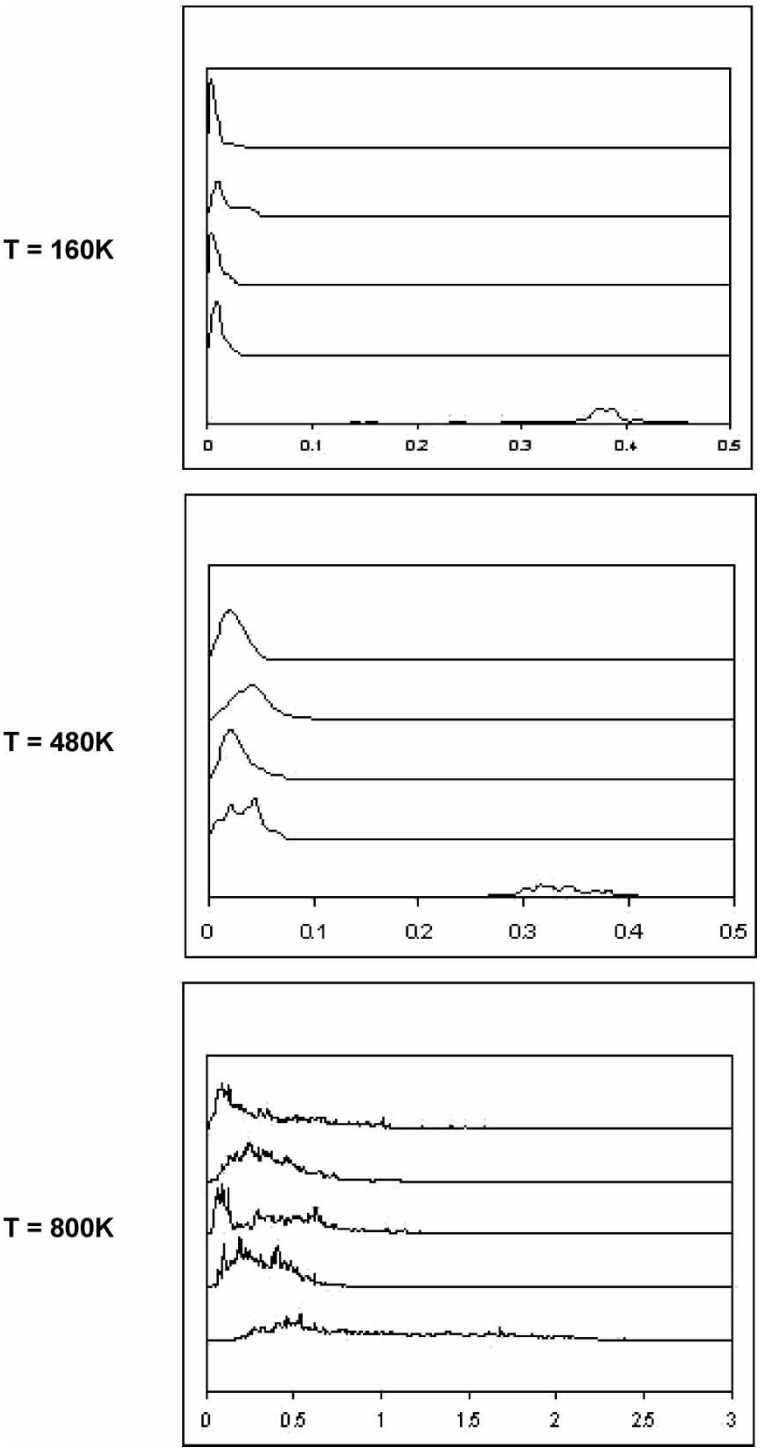

Figure 2. Radial distributions for He, Ne, Ar, Kr and Xe (bottom to top in each plot) at $T = 160$, 480 and 800 K. Vertical axes are in arbitrary units and horizontal axes are atom–atom separation in Ångstrom. To demonstrate high-temperature behavior adequately, the $T = 800$ K horizontal axis is expanded relative to the others.

the geometrical center of the Fullerene cage. Figure 6 shows the He–He separation distribution at representative low and high temperatures for various number of encapsulated atoms. The separation distribution is the probability that the He–He separation r_{ij} is somewhere between r_{ij} and $r_{ij} + \Delta r_{ij}$. In figures 5 and 6, the dependence of the distributions on particle number (N for the radial distribution and $1/2N(N-1)$ for the separation distribution) has not been normalized out because of graphical considerations.

There is considerable difference between the single and multiple He results, indicating the presence of a high degree of stress for constituents of the latter case. It is interesting to note that in both the high and low temperature cases both the radial and separation distributions show structure, as they are not flat. In addition, behavior of the radial and separation

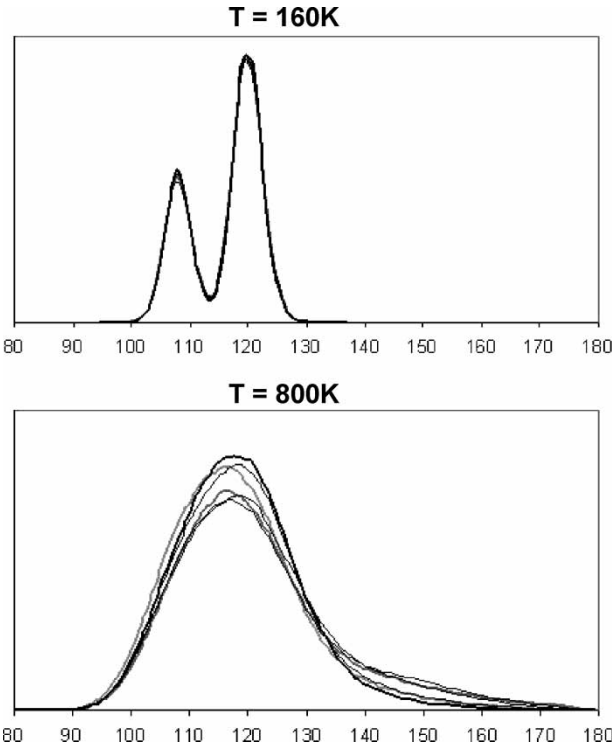

Figure 3. Carbon atom bond-angle distributions for the empty cage (lower gray), He (upper gray), Ne (bold), Argon (highest regular black), Krypton (regular black) and Xe (regular black) at $T = 160\,\mathrm{K}$ (top) and $T = 800\,\mathrm{K}$ (bottom). Vertical axes are in arbitrary units and horizontal axes are angles in degrees.

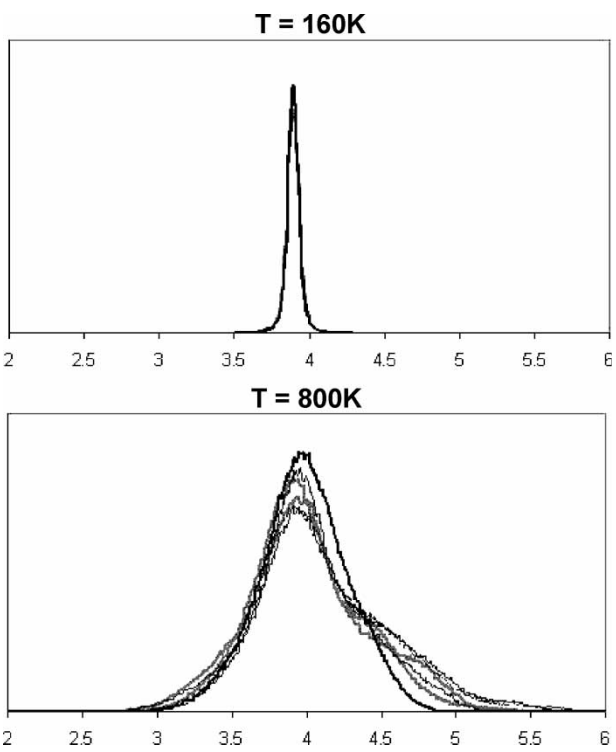

Figure 4. Carbon atom radial distributions for all cases of single-atom encapsulation as well as for the empty cage at $T = 160\,\mathrm{K}$ (top) and $T = 800\,\mathrm{K}$ (bottom). The format is identical to that of Figure 3, except that the horizontal axes are atomic position in Ångstroms.

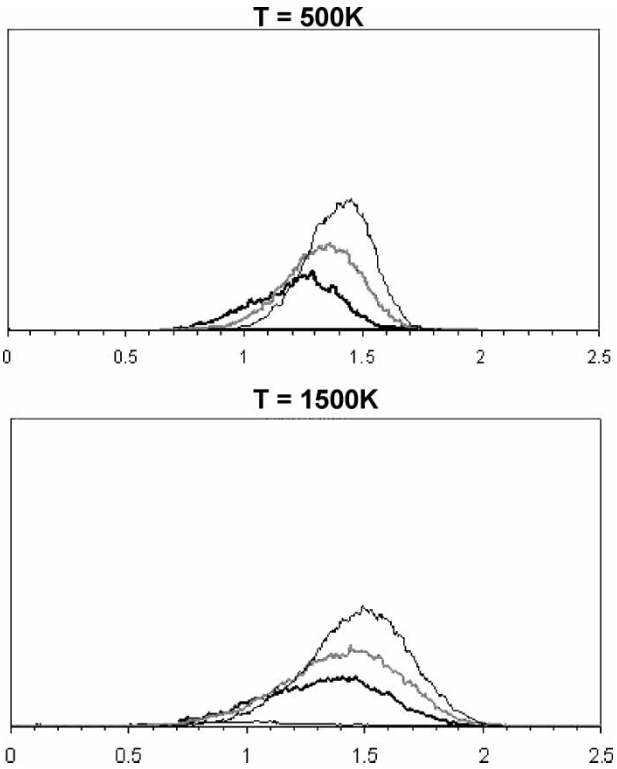

Figure 5. Radial distributions for 2 (bold, bottom), 3(gray) and 4 (black, top) encapsulated He atoms at $T = 500\,\mathrm{K}$ (upper plot) and $T = 1500\,\mathrm{K}$ (lower plot). Vertical axes are in arbitrary units and horizontal axes are atomic positions in Ångstroms. All scales are identical and the dependence (N) of the functions on particle number have not been normalized out.

distribution peaks with increasing temperature for the system clearly shows thermal expansion. The He–He separation distributions especially show that increasing temperature from $T = 500$ to $1500\,\mathrm{K}$ results in a much greater proportional change in the double and triple He systems than for quadruple He, suggesting that fluctuations for the quadruple He system are stifled due to considerable steric hindrance. Also, the radial distribution shows a much larger spread in their peak positions at $T = 500\,\mathrm{K}$ than at

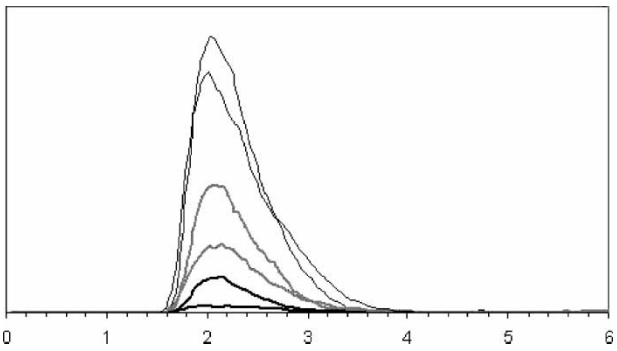

Figure 6. Helium–helium separation distributions for 2 (bold, lower pair), 3 (gray pair) and 4 (regular black, upper pair) encapsulated He atoms at $T = 500\,\mathrm{K}$ (lower curve in a pair) and $T = 1500\,\mathrm{K}$ (upper curve in a pair). Vertical axes are in arbitrary units and the horizontal axes are atom–atom separation in Ångstroms. All scales are identical and the dependence ($1/2N(N-1)$) of the functions on particle number have not been normalized out.

$T = 1500$K, where the peaks are located much closer to each other. Such observations are consistent with the observation that placing four He atoms inside the cage is approaching the limit of packing. Even though thermal expansion is evident in the encapsulated system, there does not appear to be a phase transition in over a 1000K temperature range. It could be that phase transitions in such highly stressed systems exhibit novel properties, and certainly warrant further investigation.

As with single-atom encapsulate simulations, some aspects of temperature control here must also be emphasized: unlike for single atom encapsulates, here the temperatures of the He "molecule" and the Fullerene cage are controlled separately. As a result, the "temperature" of the encapsulate has some significance for multiple He systems, although very small ones. Such temperature control may be partly responsible for the large difference in the behavior of single and multiple encapsulated systems in the simulations reported here, but we suspect that the conclusions reached about the fundamental dynamics exhibited will not change significantly.

There seem to be minimal effects on the cage structure from placing different numbers of He atoms within it. However, comparison of relative heights and widths of the carbon atom radial distributions suggest that at higher temperatures the cage is most disrupted in the single He case and that incorporation of more that one He tends to stabilize the system, even in comparison to the empty cage case.

Acknowledgements

The first author gratefully acknowledges discussions with J. Che and R.J. Cross. All authors are grateful to the University of Northern Iowa for partial support of this work through summer 2002 undergraduate research fellowships.

References

[1] L. Becker, R.J. Poreda, T.E. Bunch. Fullerenes: An extraterrestrial carbon carrier phase for noble gases. *PNAS*, **97**(7), 2979 (2000).

[2] M. Saunders, R.J. Cross. Putting nonmetals into Fullerenes. In *Endofullerenes*, T. Akasaka, S. Nagase (Eds.), Kluwer, Dordrecht (2002), and references contained therein.

[3] M. Saunders, R.J. Cross, H.A. Jiménez-Vázquez, R. Shimshi, A. Khong. Noble gas atoms inside Fullerenes. *Science*, **271**, 1693 (1996) and references contained therein.

[4] M.S. Syamala, R.J. Cross, M. Saunders. ^{129}Xe NMR spectrum of Xenon inside C_{60}. *J. Am. Chem. Soc.*, **124**, 6216 (2002).

[5] R.J. Cross, A. Khong, M. Saunders. Using Cyanide to put noble gases inside C_{60}. *J. Org. Chem.*, **68**(21), 8281 (2003).

[6] T. Sternfeld, R.E. Hoffman, M. Saunders, R.J. Cross, M.S. Syamala, M. Rabinovitz. Two helium atoms inside Fullerenes: Probing the internal magnetic field in C_{60}^{6-} and C_{70}^{6-}. *J. Am. Chem. Soc.*, **124**, 8786 (2002).

[7] J. Laskin, T. Peres, C. Lifshitz, M. Saunders, R.J. Cross, A. Khong. An artificial molecule of Ne_2 inside C_{70}. *Chem. Phys. Lett.*, **285**, 7 (1998).

[8] T. Weiske, H. Schwarz, D.E. Giblin, M.L. Gross. High-energy collisions of $Kr@C_{60}^{+}$ with helium: evidence for the formation of $HeKr@C_{60}^{+}$. *Chem. Phys. Lett.*, **227**, 87–90 (1994).

[9] E. Sanville, J.J. DelBruno. Computational studies of possible transition structures in the insertion and windowing mechanisms for the formation of endohedral fullerenes. *J. Phys. Chem. B*, **107**, 8884 (2003).

[10] S. Patchkovskii, W. Thiel. How does helium get into buckministerfullerene? *J. Am. Chem. Soc.*, **118**, 7164 (1996).

[11] T.-H. Feng, W.-J. Chang. Phase transformations of Fullerenes using molecular dynamics simulations. *Microelectr. J.*, **35**, 581 (2004).

[12] S.G. Kim, D. Tomanek. Melting the Fullerenes: a molecular dynamics study. *Phys. Rev. Lett.*, **72**(15), 2418 (1994).

[13] B.L. Zhang, C.Z. Wang, C.T. Chan, K.M. Ho. Thermal disintegration of carbon Fullerenes. *Phys. Rev. B*, **48**(15), 11381 (1993).

[14] R.T. Chancey, L. Oddershede, F.E. Harris, J.R. Sabin. Fragmentation of Fullerenes. *Phys. Rev. A*, **67**, 043203 (2003).

[15] A. Martinez-Alonso, J.M.D. Tascon, E.J. Bottani. Physical adsorption of Ar and CO_2 on C60 Fullerene. *J. Phys. Chem. B*, **105**, 135 (2001).

[16] Y. Yamaguchi, S. Maruyama. *ICHMT Symposium Molecular & Microscale Heat Transfer*, Yokohama (1996), Dec. 1–5.

[17] S. Maruyama, Y. Yamaguchi. A molecular dynamics of the formation process of Fullerene. *Trans. JSME Ser. B*, **63–611**, 2405 (1997).

[18] Y. Yamaguchi, S. Maruyama. A molecular dynamics simulation of the Fullerene formation process. *Chem. Phys. Lett.*, **286**, 336 (1998).

[19] S. Maruyama, Y. Yamaguchi. A molecular dynamics demonstration of annealing to a perfect C_{60} structure. *Chem. Phys. Lett.*, **286**, 343 (1998).

[20] Y. Yamaguchi, S. Maruyama. A molecular dynamics of the formation process of Fullerene. *Trans. JSME Ser. B*, **63–611**, 2398 (1997).

[21] D.W. Brenner. Empirical potential for hydrocarbons for use in simulating the chemical vapor deposition of diamond films. *Phys. Rev. B*, **42**(15), 9458 (1990).

[22] J. Che, T. Çagin, W.A. Goddard. Studies of Fullerenes and carbon nanotubes by an extended bond order potential. *Nanotechnology*, **10**, 263 (1999).